INTERNATIONAL JOURNAL OF INTEGRATED ENGINEERING
ISSN: 2229-838X e-ISSN: 2600-7916

IJIE

Vol. 17 No. 9 (2025) 285-296
https://publisher.uthm.edu.my/ojs/index.php/ijie

Comparison of Myocardial Mechanical Metrics in Electromechanical Model vs. Fluid-Electromechanical Model

Azam Ahmad Bakir[1]*, Mohd Jamil Mohamed Mokhtarudin[2]

[1] *Smart Manufacturing and Systems Research Group, University of Southampton Malaysia, 79100 Iskandar Puteri, Johor, MALAYSIA*
[2] *Centre for Research in Advanced Fluid and Processes (Fluid Centre), Universiti Malaysia Pahang Al-Sultan Abdullah, Lebuhraya Tun Razak, 26300 Kuantan, Pahang, MALAYSIA*

*Corresponding Author: a.ahmad-bakir@soton.ac.uk
DOI: https://doi.org/10.30880/ijie.2025.17.09.019

Article Info

Received: 11 May 2025
Accepted: 15 August 2025
Available online: 31 December 2025

Keywords

Heart modelling, heart electromechanics, blood haemodynamics, heart finite element model

Abstract

The development of multiphysics heart model has grown tremendously over the past decade. In this paper, we compare two multiphysics approaches: electromechanics and fluid-electromechanics, in simulating left ventricular mechanics and the output of mechanical metrics. Cardiac electromechanical (EM) model refers to the approach of simulating heart mechanical deformation, triggered by cardiac action potential, while the generated ventricular pressure is determined by a penalty function and applied uniformly across the endocardium. Fluid-electromechanics (Fluid-EM) approach relies on similar action potential wave to trigger mechanical deformation but the ventricular pressure is determined by solving the Navier-Stokes equations within the ventricular cavity. Thus, Fluid-EM is more accurate as it models the two-way blood-ventricular interaction, producing more realistic loading on the endocardium and enabling analysis of ventricular blood flow dynamics. Due to its complexity, the Fluid-EM approach is more computationally demanding than the EM approach. We assessed several mechanical metrics within the ventricle namely stresses and strains to assess regional differences in the heart by implementing both approach in a heart geometry extracted from a healthy patient. Differences in the mechanical metrics were noted indicating both models were loaded differently due to differences in modelling the blood. This suggests that in greater differences can be expected should there be more regional differences in the myocardium such as in infarct cases.

1. Introduction

Computational study has been increasingly useful in complementing physical experiments in answering crucial cardiac research questions. Cardiac muscle involves interaction of different physical domains where the electrical action potential triggers muscle contraction and in turns help eject the blood into the circulation. While simulating these interactions offer greater model fidelity, it can be time consuming and computationally expensive to develop and run. Therefore, some simplifications along with assumptions are necessary to develop a workable model.

In earlier models of ventricular motion, the entire ventricle is assumed to contract uniformly by the contraction of all the cardiac muscles at the same time [1]. In reality, cardiac activation follows a certain sequence, which helps to optimize pumping mechanism [2]. The endocardium is applied with the ventricular pressure,

determined by the afterload, obtained via the Windkessel circulation and atrial pressure [3]. With electromechanical model, the effect of electrical activation propagation across ventricles can be simulated, opening possibility of studying the impact of abnormalities in cardiac activation on mechanical performance [3-5]. The incorporation of this electrical and mechanical model opens avenue to study diseases such as myocardial infarction [6, 7]. fibrillation, and cardiac dyssynchrony while enabling medical device optimization study such as placement of lead in resynchronization therapy [8]. More recently, the incorporation of Navier-Stokes equations to simulate blood flow dynamics has been increasingly common. These added capabilities to observe mechanical impact on the flow pattern as well as interaction with internal structure such as valves [9] or septal defects [10].

Understanding the change in flow pattern provides a new development in disease diagnosis and development of prosthesis such as artificial valves and cardiac patches. Nonetheless, combining Navier-Stokes equations with electromechanical model of the heart is rarely applied due to complexity of the equations and often necessitates large computing power. The mechanical deformation of the heart, triggered by the action potential, helps to squeeze the blood and ejects it out to the entire circulation system. Once the muscle relaxes, the mitral valve opens and the blood rushes into the chamber, expanding the myocardium for the next cardiac cycle. As such, the inclusion of Navier-Stokes provides a more accurate representation of heart physics.

In this study, we compare the mechanical metrics generated by two different approaches in cardiac modelling, electromechanical alone (EM) and electromechanically driven fluid-structure interaction model (EM-FSI). In EM model, pressure load is applied uniformly on the endocardium of the ventricles while EM-FSI produces a heterogenous loading depending on regional fluid total stress. To the best of our knowledge, the comparison of both approaches had been scarcely investigated. Using Navier-Stokes equations, a more realistic load can be simulated by the contribution of both fluid pressure and viscous stress due to the flow, which constitutes the fluid total stress. It is expected that the mechanical metrics will be different in both approaches since the fluid load in EM-FSI is heterogenous across the endocardium or the inner wall of the heart. We assess mechanical metrics such as pressure-volume relations, mechanical torsion, regional work, as well as stress and strains.

2. Methods

2.1 Geometry

The geometry was extracted from CT-Scan images of a healthy patient, available online via an open-source website (SimVascular.com). We segmented the images into a 3D myocardial geometry using open-source tool 3DSlicer (3DSlicer.org). The segmented aortic artery geometry was available on the website and later merged with the myocardial geometry in COMSOL Multiphysics 6.1 (COMSOL A.B. Sweden) geometry tool. For EM model, the aortic geometry was not included as the fluid compartment is not modelled. Myocardial microstructure, namely, fibre, sheet and normal-to-sheet orientations were defined by using Poisson-type formulation approached as described by [11]. The fibre is set to be -60 degrees relative to the circumferential orientation at the epicardium (outer surface) and 60 degrees in the endocardium (inner surface) as shown in Fig. 1 (c). The sheet is assumed to be oriented radially across the wall thickness whilst the normal-to-sheet is assumed to be orthonormal to both fibre and sheet.

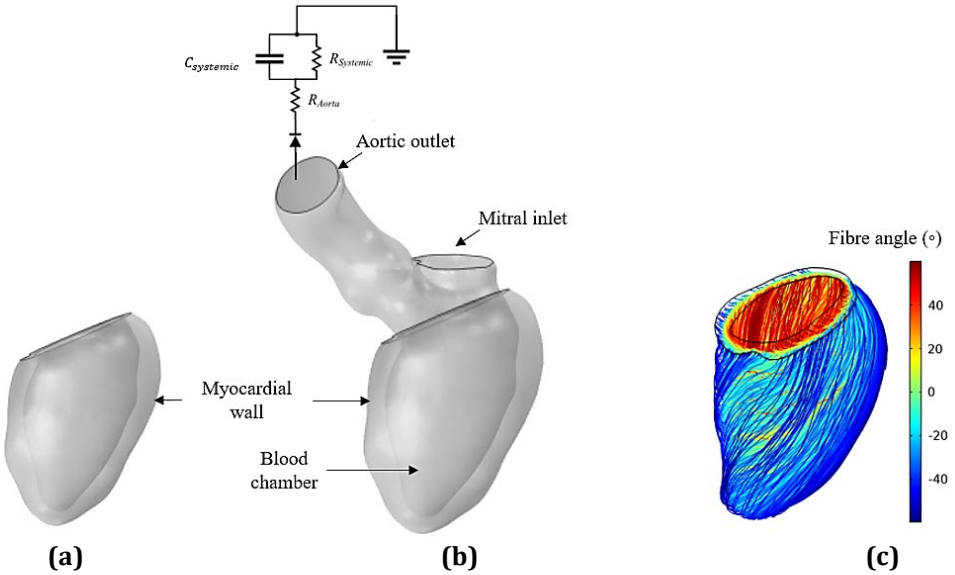

Fig. 1 *(a) The geometry for EM model, where blood domain is not simulated; (b) Geometry for EM-FSI model, with inlet and aortic tract visible; (c) Orientation of defined muscular fibre angle relative to the circumferential direction*

2.2 Electromechanical formulation

Electromechanical formulations have been described extensively in these works [12-14]. In general, a phenomenological action potential model is utilized to describe the momentary spike of myocardial electric potential. The formulations consist of two variables, namely the membrane potential, V, and relaxation variable, R as shown in equations (1-3). Electrical conductivity is assumed to be orthotropic where it is most conductive along the fibre $\hat{F}$, followed by the sheet, $\hat{S}$, and the normal-to-sheet, $\hat{N}$. Thus, the electrical conductivity tensor is presented in Equation 4.

$$\beta\left(C_m\frac{\partial V_m}{\partial t}+i_{ion}\right)=\nabla_X.(\boldsymbol{\sigma}\nabla_X V_m) \tag{1}$$

$$i_{ion}=k_1k_2(V_m-B)\left(\left[\frac{V_m-B}{A}-a\right](V_m-1)+k_2R(V_m-B)\right. \tag{2}$$

$$\frac{\partial R}{\partial t}=\left(\varepsilon_0+\frac{\mu_1 R}{\left[\frac{V_m-B}{A}\right]+\mu_2}\left(-R-k_1\left[\frac{V_m-B}{A}\right]\left(\left[\frac{V_m-B}{A}\right]-a-1\right)\right)\right. \tag{3}$$

$$\boldsymbol{\sigma}=\sigma_f\left(\hat{F}\otimes\hat{F}\right)+\sigma_s\left(\hat{S}\otimes\hat{S}\right)+\sigma_n\left(\hat{N}\otimes\hat{N}\right) \tag{4}$$

The membrane potential, V, triggers the activation of active mechanical stress, T_a, by the following equation, which produced an isometric tension when V rises. This phenomenological active stress is governed by following ordinary differential equation in Equation 5 and activation function in Equation 6. The active stress is coupled to the myocardial mechanics by adding the term to the 2nd Piola Kirchoff Stress, **T** as shown in Equation 7. A cross-fibre active stress of 40% Ta was added based on [15]. This provides active deformation to the myocardium, whilst the passive myocardial property is governed by a transversely isotropic hyperelastic strain-energy function, developed by Holzapfel-Ogden (2009), shown in Equation 8 [16]. The parameters for each parameters are available in the original work (Bakir et al. 2018) and listed in Table 1 [13]. **E** for Equation 8 refers to Green-Lagrange strain, I_1 is first invariants of the isochoric elastic right Cauchy-Green tensor, **C** whilst $I_{4f}=\hat{F}\cdot(\mathbf{C}\hat{F})$. J denotes the determinants of deformation gradient tensor, **F**.

$$\frac{\partial T_a}{\partial t}=\epsilon(V_m)\left(k_{Ta}\left[\frac{V_m-B}{A}\right]-T_a\right) \tag{5}$$

$$\epsilon(V_m)=\epsilon_0+(\epsilon_\infty-\epsilon_0)exp\left(-exp\left(-\xi(V_m-V_{threshold})\right)\right) \tag{6}$$

$$\mathbf{T}=\frac{\partial\psi}{\partial\mathbf{E}}+T_a\left(\hat{F}\otimes\hat{F}\right)+0.4T_a\left(\hat{S}\otimes\hat{S}\right)+0.4T_a\left(\hat{N}\otimes\hat{N}\right) \tag{7}$$

$$\psi=\frac{a_i}{2b_i}exp(b(I_1-3)-1)+\frac{a_f}{2b_f}exp\left(b_f\left(I_{4f}-1\right)^2-1\right)+\frac{\kappa(J-1)ln(J)}{2} \tag{8}$$

2.3 Left ventricular pressure formulation for EM model

The model was run in a purely electromechanical setting where the Navier-Stokes equations were not implemented. This mode of simulation was performed to compare EM-FSI model behavior against the more common approach in which the endocardium is applied with a spatially uniform left ventricular pressure, P_{LV} from Eq.10). In this mode of simulation, the fluid domain was removed as it was no longer necessary. The P_{LV}, during the isovolumic phases was determined as in Eq. 9 based on work by Usyk et al (2002) [17].

$$P_{LV,iso}=P_{LV,previous}+k_b(V_{LV,previous}-V_{LV}) \tag{9}$$

where, k_b is the proportionality constant set to 1000 mmHg/ml to control the pressure needed to maintain a certain volume. This value was found sufficient to obtain the isovolumic phases of the LV. $P_{LV,previous}$ and

$V_{LV,previous}$ are the pressure and volume of the previous time step respectively. The LV pressure for the whole cardiac cycle was governed by the following relation:

$$P_{LV} = \begin{cases} P_{systemic} + Q_{aorta}\, R_{aorta} & P_{LV,iso} > P_{systemic} \\ P_{LV,iso} & P_{LV,iso} \leq P_{systemic}\ and\ P_{LV,iso} \geq P_{LA} \\ P_{LA} + Q_{mitral}\, R_{mitral} & P_{LV,iso} < P_{LA} \end{cases} \quad (10)$$

where $P_{systemic}$ is given by the three-element Windkessel in Eq. 15 while Q_{aorta} and Q_{mitral} and is the time-derivative of LV volume, V_{LV}.

2.4 Additional Formulations for EM-FSI

In the EM-FSI model, the inner cavity, housing the blood, is governed by the conservation of mass and conservation of momentum, also known as the Navier-Stokes equations. We assumed the blood as incompressible and laminar and Newtonian fluid for simplicity. The system is set as a two-way coupled interaction where the blood exerts the fluid pressure and the total stress onto the endocardial wall, while the deformation of the wall exerts change in fluid wall velocity.

$$\rho_f \frac{\partial u_f}{\partial t} + \rho(u_f \cdot \nabla)u_f = \nabla \cdot \left[-p\mathbf{I} + \mu(\nabla u_f + (\nabla u_f)^T)\right] \quad (11)$$

$$\rho_f \nabla \cdot u_f = 0 \quad (12)$$

where u_f and p, are the blood velocity vector and pressure respectively. The mitral valve inlet is set to a fully developed flow rate, Q_{mitral}, determined by constant left atrial pressure of 12 mmHg. The aortic outlet flow rate, Q_{aorta}, is determined by a three-element Windkessel to govern its afterload, imposed by external circulation. Q_{aorta} is then applied as a fully developed flow rate condition to the aortic outlet. All parameters are available in Table 1, as taken from [13, 18] . The rest of the wall is set with no-slip boundary conditions.

$$Q_{mitral} = \begin{cases} \frac{P_{LA} - P_{LV,mitral}}{R_{mitral}}, & P_{LA} > P_{LV,mitral} \\ 0, & P_{LA} \leq P_{LV,mitral} \end{cases} \quad (13)$$

$$Q_{aorta} = \begin{cases} \frac{P_{LV,aorta} - P_{systemic}}{R_{Aorta}}, & P_{LV,aorta} > P_{systemic} \\ 0, & P_{LV,aorta} \leq P_{systemic} \end{cases} \quad (14)$$

$P_{systemic}$ is determined from Windkessel ODE:

$$Q_{aorta} = C_{systemic} \frac{dP_{systemic}}{dt} + \frac{P_{systemic}}{R_{systemic}} \quad (15)$$

where $P_{LV,mitral}$ and $P_{LV,aorta}$ are the average pressure at mitral inlet and aortic outlet respectively.

A moving mesh formulation is used to govern the mesh deformation of the inner cavity where a pseudo-hyperelastic Yeoh function is used to govern the mesh deformation, with Yeoh stiffening factor set to 100. The full formulation and parameters are s available in our previous work [13]. The fluid-solid boundary, where the myocardial wall and blood interacts, is set to have similar displacement. The aortic tract and mitral inlet domains were set as rigid.

Int. Journal of Integrated Engineering Vol. 17 No. 9 (2025) p. 285-296

Table 1 *List of model parameters*

Parameter	Value [unit]	Description
β	160000 [1/m]	Cell surface-to-volume ratio
C_m	1[uF/(cm^2)]	Cell capacitance
k_1	8 [1]	Action potential parameter
k_2	0.1 [1/ms]	Action potential parameter
B	-0.08 [V]	Membrane potential scaling
A	0.1 [V]	Membrane potential scaling
ε_0	0.0002[1/ms]	Action potential parameter
μ_1	0.02[1/ms]	Action potential parameter
μ_2	0.3[1]	Action potential parameter
a	0.12	Membrane potential scaling
σ_f	0.015 [S/m]	Electrical conductivity in fibre direction
σ_s	$0.5 * \sigma_f$	Electrical conductivity in sheet direction
σ_n	$0.25 * \sigma_f$	Electrical conductivity in normal-to-sheet direction
k_{Ta}	170 [kPa]	Isometric muscle stress
ϵ_0	0.00045 [1/ms]	Active stress parameter
ϵ_∞	0.03 [1/ms]	Active stress parameter
$V_{threshold}$	-0.03 [V]	Active stress parameter
a_i	2.280[kPa]	Tissue stiffness parameter
b_i	9.726	Tissue stiffness parameter
a_f	1.685[kPa]	Tissue stiffness parameter along fibre
b_f	15.779	Tissue stiffness parameter along fibre
κ	250 [kPa]	Bulk modulus
R_{aorta}	0.05 [mmHg*s/ml]	Aortic valve resistance
R_{mitral}	3.47e6 [Pa*s/(m^3)]	Mitral valve resistance
ρ_f	1060 [kg/m^3]	Blood density
μ	3.5e-3 [Pa*s]	Blood viscosity
P_{LA}	12 [mmHg]	Atrial pressure
$C_{systemic}$	3 [ml/mmHg]	Systemic circulation capacitance
$R_{systemic}$	1.15[mmHg*s/ml]	Systemic circulation capacitance
ξ	10 [1/V]	Active stress parameter

2.5 Model settings

The model is run as fully coupled in COMSOL Multiphysics 6.1 (COMSOL A.B. Sweden) using second-order BDF time-marching solver. Output time step and maximum time step is set to 2 ms. Extrasystole electrical stimulus was applied at the endocardial surface at time t = 2 ms. The model was run for 3 cycles until stability of the results. Analysis is performed at the third cycle. We used default "normal" mesh setting in COMSOL for this preliminary assessment. A total of 63610 mesh elements were built for EM-FSI model with 0.7 cm average mesh size in solid domain and 0.47 cm for fluid domain. 4193 elements were built for EM model 0.95 cm average mesh size. Do note that the mesh for EM-FSI is slightly smaller in myocardium because of fine boundary layer mesh at the interface. A mesh independence study was held on the myocardium, looking at myocardial apex displacement as index for mesh independence. The results compared against Finer setting (14017 element in myocardium with average mesh size of 0.6 cm) showed less than 2% difference in time-averaged apex displacement. Overall, it took 1 day 15 hours, 54 minutes to run the EM-FSI, while it took only 1 hour 2 min 14 s on the EM model on an Intel i7-8700 3.20 GHz machine with 32 Gb RAM.

3. Results and Discussion

Upon application of stimulus at t = 2 ms, the action potential spreads from the inner surface (endocardium) towards the outer surface (epicardium). As the myocardium is activated, the heart muscle twists and the inner cavity volume is squeezed out, indicating the blood ejection phase. As the muscle relaxes, the myocardium gradually returns to the original stage as the blood is being filled up. Looking at the pressure-volume relation of the blood cavity, it can be seen a "box" shape plot was achieved, indicating a typical cardiac cycle. However, slight differences can be observed for EM-FSI where ejection fraction is slightly lower, and ejection pressure is slightly higher than the EM model. This can be attributed to the extra flow resistance imposed in EM-FSI by the aortic outlet and aortic tract, which is not considered in the EM model. Furthermore, some noise can be observed in EM-FSI likely due to flow oscillation. This additional resistance can be difficult to quantify as it can be greatly dependent on patient-specific geometry and wall stiffness, of which resistance can be greatly influenced [19].

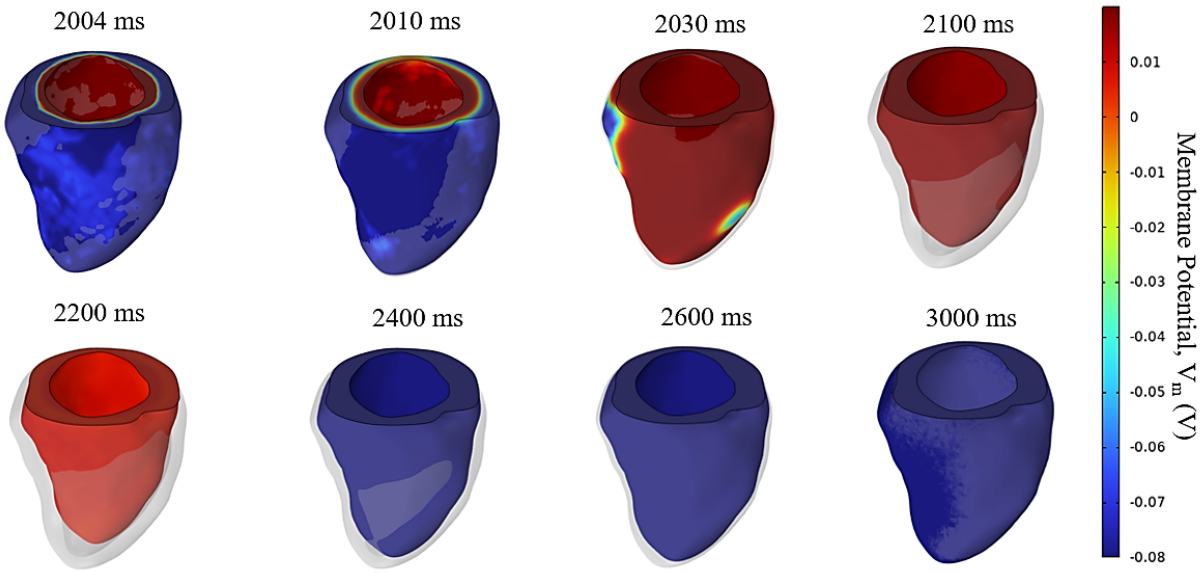

Fig. 2 *The time-course of membrane potential (Vm) and general deformation of myocardium at third cycle. Gray outline indicates the end-diastolic shape. Peak ejection occurs at t = 2100 ms and peak filling phase occurs at 2400 ms*

The advantage of running the EM-FSI model vs EM model is it can provide spatial information on blood pressure and blood velocity. This can be seen in Fig. 3 and Fig. 4 describing the distribution of pressure and velocity in the blood domain. Such information can be crucial in investigating implant interaction with the blood. Fig. 3 shows the distribution of blood pressure in the blood domain. A large pressure range is noted initially following the stimulus possibly due to the sudden movement of the myocardium to initiate contraction, until the start of ejection (t = 2030 ms). At peak ejection (t = 2100 ms), the range of blood pressure is large at nearly 30 mmHg, however, most of the pressure variation is at the aortic tract, while the pressure is quite uniform within the ventricle. In the filling phase, blood pressure variation is minuscule, often less than 1 mmHg. The streamline of blood velocity can also be simulated with EM-FSI model where a nearly straight streamline can be seen at peak ejection while vortices can be seen forming at peak filling phase. These vortices have been proposed as key measure to diagnose diastolic function of the heart, which can be accessed via non-invasive echocardiogram [18].

Int. Journal of Integrated Engineering Vol. 17 No. 9 (2025) p. 285-296

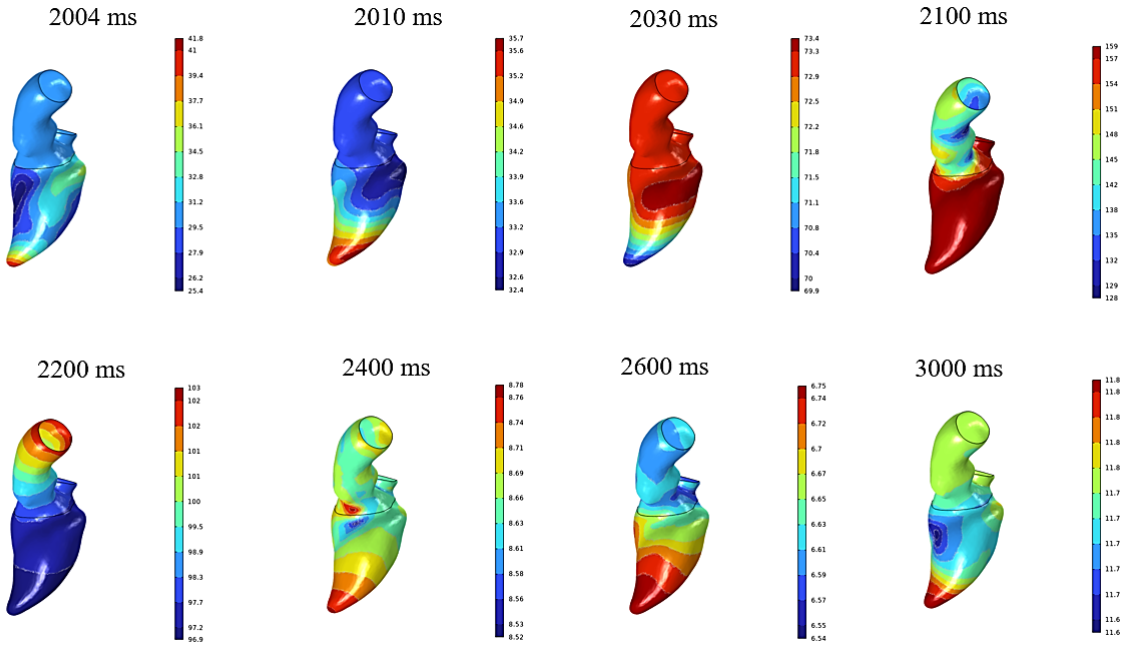

Fig. 3 *Time course of fluid pressure within the ventricle at third cycle*

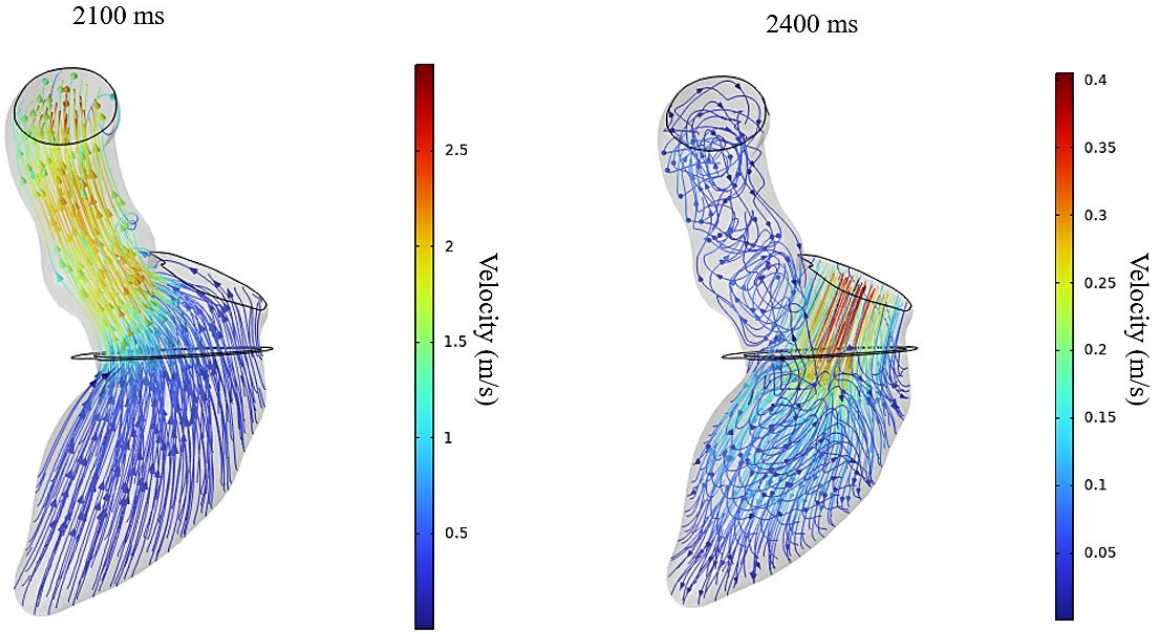

Fig 4 *Fluid streamlines at peak ejection (t =2100 ms) and peak filling phase (t=2400 ms)*

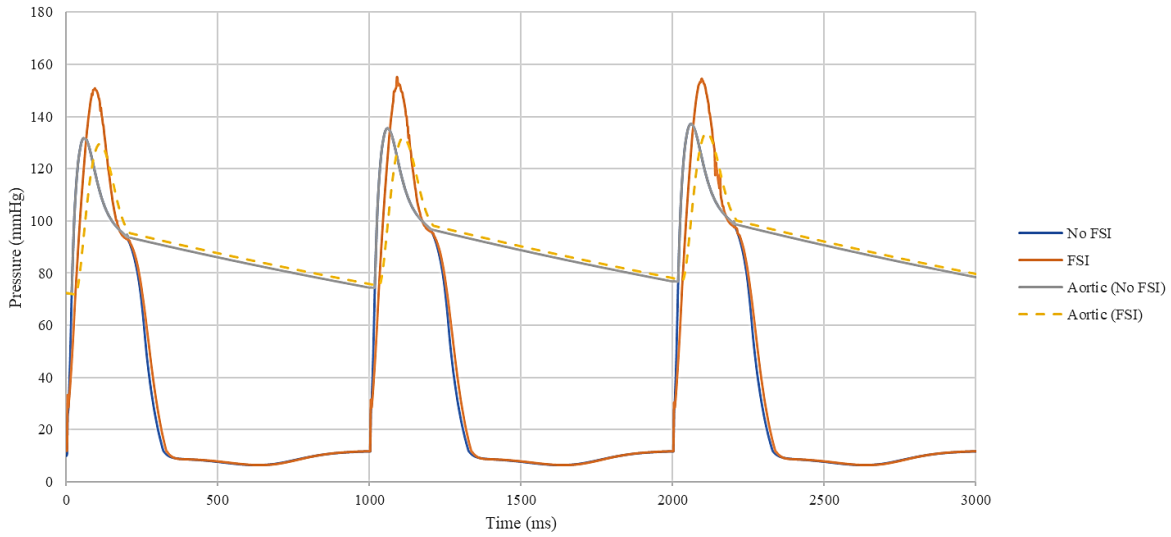

Fig. 5 *Internal LV pressure and aortic pressure over three cardiac cycles.*

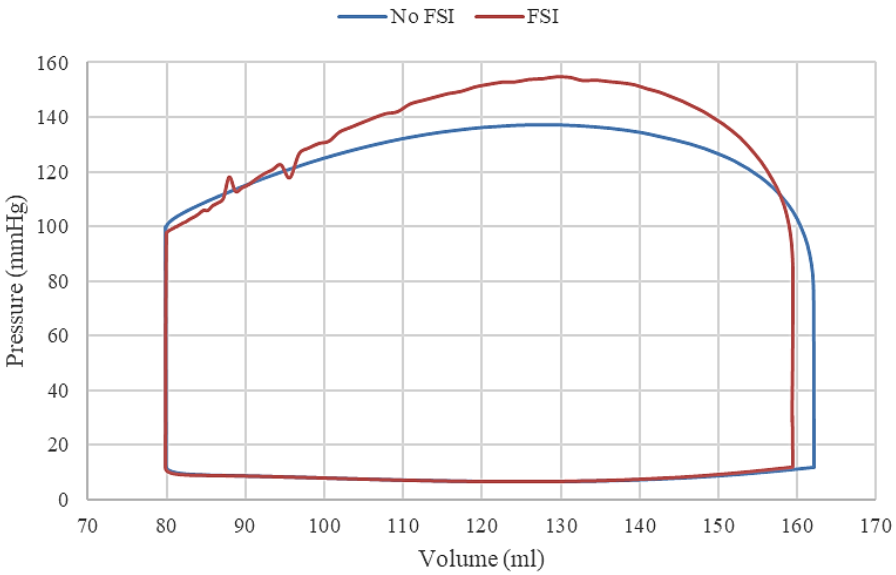

Fig 6 *Pressure-volume taken at third cycle for both EM and EM-FSI model*

By looking at global mechanical metrics such as apex displacement and myocardial torsion (or twist), some differences can also be observed. Both metrics are commonly used to assess global mechanical function of the heart and can be easily quantified view echocardiogram. Apex displacement is measured by placing a point probe at the bottom-most or apex of the heart, and the total upward displacement was measured. Torsion was measured by calculating the twist at the apex relative to the base, with zero twist considered at the end-diastole (t = 0). Negative torsion indicates a counterclockwise twist, which is common in the heart due to larger mass of outer surface muscle, contributing to greater counterclockwise moment. The amount of apex displacement and torsion are comparable to what observed in healthy human heart [20]. Comparing EM and EM-FSI, some phase shift can be observed in both plots, with EM-FSI showing slightly higher peak magnitude. These phase-shifts are likely due to the need for initial pressure build-up in the EM-FSI model. A spike is also observed following the stimulus in EM-FSI model, likely caused by redistribution of fluid as the wall is contracting.

Int. Journal of Integrated Engineering Vol. 17 No. 9 (2025) p. 285-296

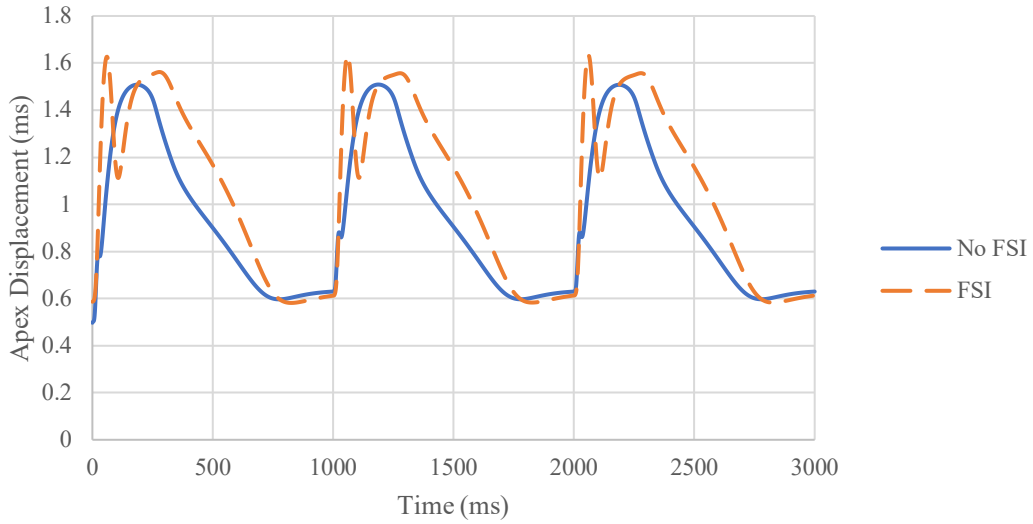

Fig. 7 *Apex displacement comparison between EM and EM-FSI models*

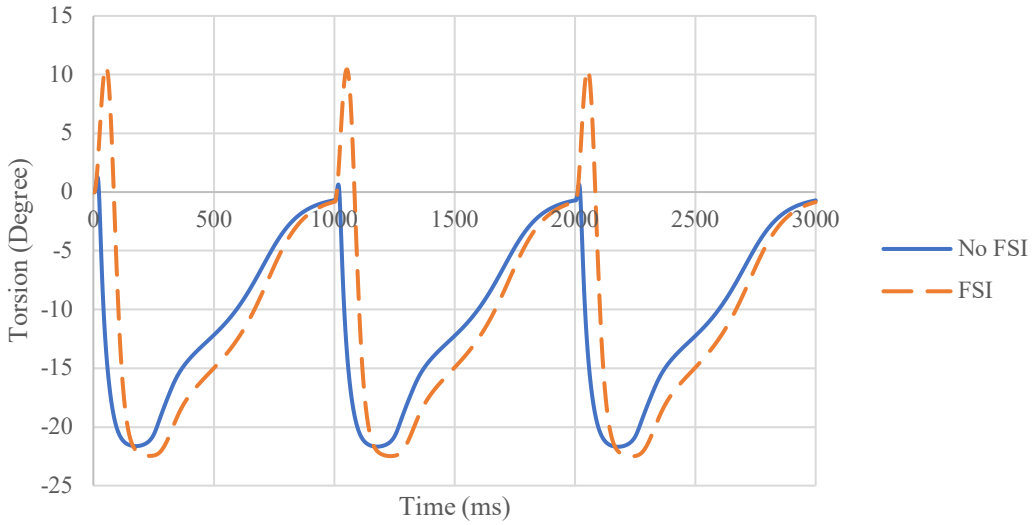

Fig. 8 *Myocardial torsion comparison between EM and EM-FSI models*

To assess local stress and strain, we extract fibre stress and fibre strain data from one point at the LV free wall and one point at septum, taken midway between the apex and base (top) of the heart as shown in Fig. 9. The stress and strain waveforms, despite showing similar shapes, have some phase-shift and magnitude differences, similar to what we observed earlier in pressure plot. The phase shift and initial spike in EM-FSI could be due to redistribution of blood in early phase of contraction. Higher magnitude is observed in EM model, possibly due to uniform pressure being applied while in EM-FSI, the more heterogenous fluid load helps to relief stress in some regions. These differences contributed to a different shape of stress-strain loop, a measure of mechanical work that correlates with heart muscle remodeling [21]. We also assess regional work of both models, calculated by the sum of product of stress and strain across the cardiac cycle. This measure is assessed at the third cycle of the model, as shown in Fig. 10. Overall, no discernable differences can be seen qualitatively. However, EM-FSI shows an elevated regional work magnitude. However, it is worth noting that this difference might be enhanced in the presence of regional mechanical differences such as presence of infarct, which is not the focus of our study.

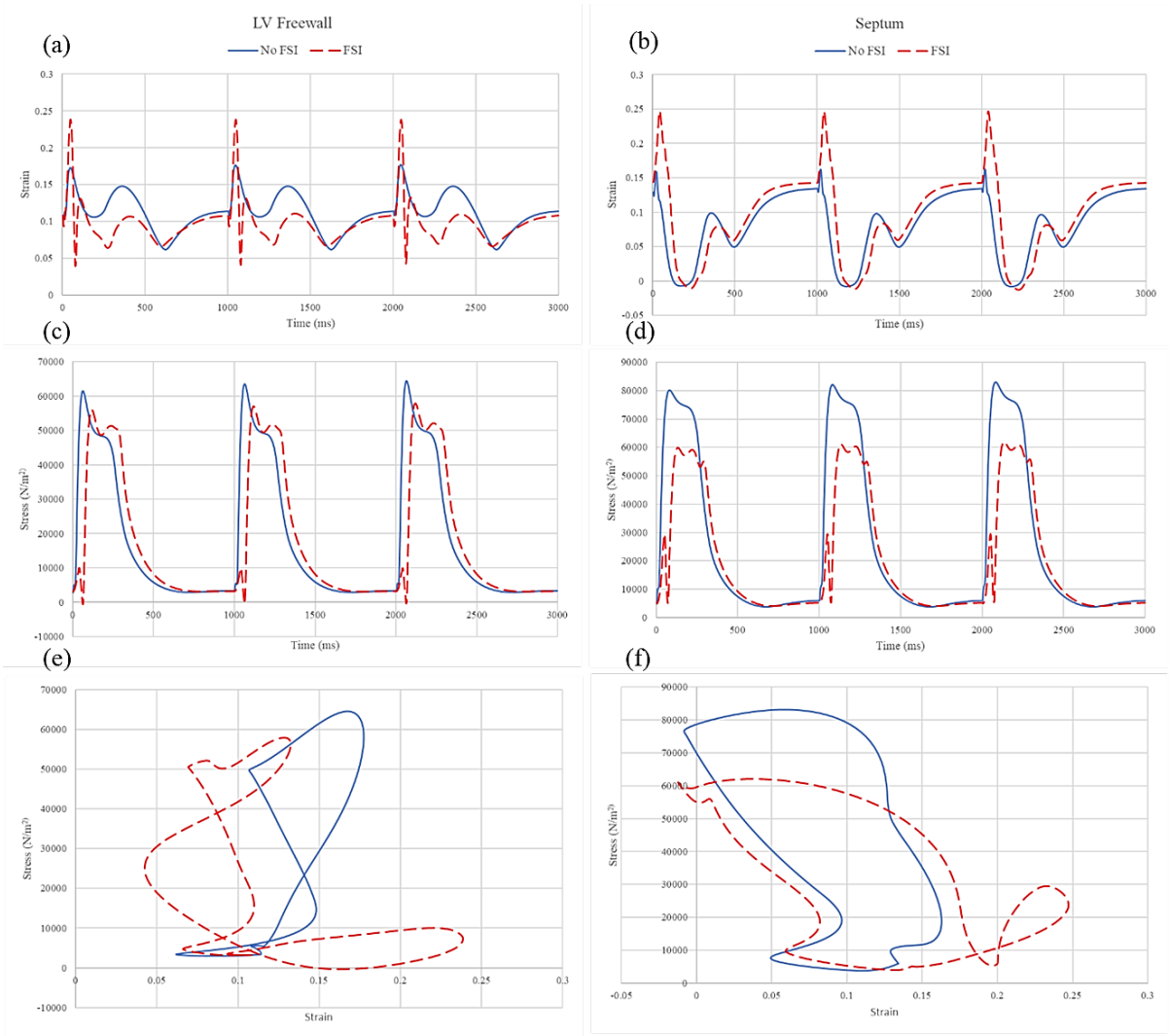

Fig. 9 *Comparison of mechanical metrics taken at a single epicardial (outer) point at LV freewall (near the mitral valve) and septum (near the aortic outlet). Measurement is taken at a distance halfway along the heart's long axis. Strain (a-b) and stress (c-d) behaviour taken at mid-point of apicobasal distance at LV freewall and septum. (e-f) Stress and strain loop for the third cycle of the heart.*

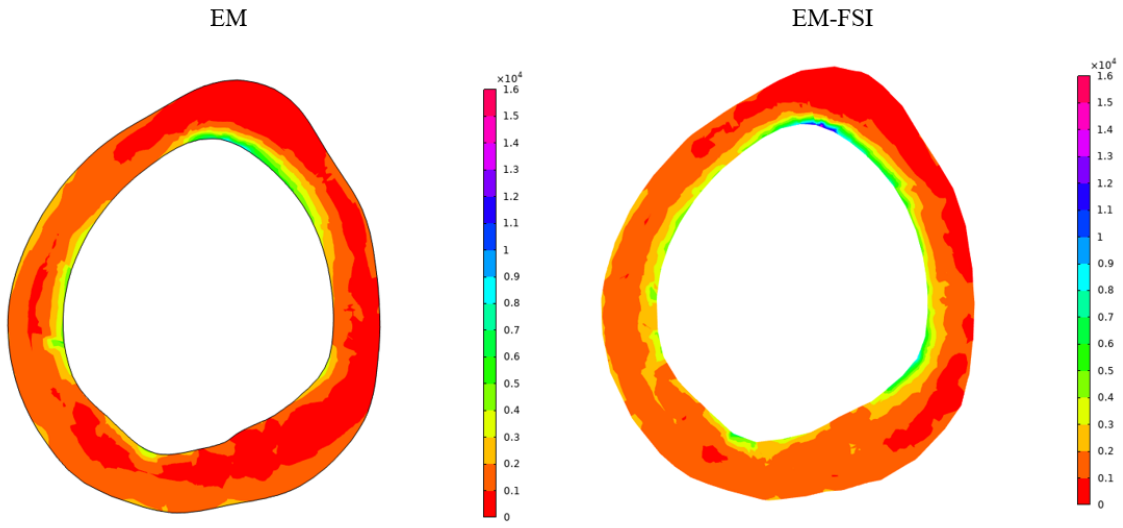

Fig. 10 *Regional work (N m^{-2}) taken at third cycle, calculated by summing the product of fibre stress and strain over the entire time cycle*

4. Limitations and Future Directions

The main advantage of using EM-FSI model is the ability to relate blood haemodynamics and myocardial mechanics, in addition to being the more accurate representation of heart physiology as it simulates the two-way interactions of heart muscle and blood. This is beneficial in assessing change in blood metrics and even modelling performance of internal implant (i.e. valve) with myocardial contraction. However, this results in higher computational cost. Whilst we are seeing some differences in the result, the general trend of both models is similar with minor changes in magnitude and some phase shift in the quantity reported. The current study was held in a healthy state model, where the entire ventricle nearly contracts in unison. Thus, it can be expected the trend might be greater in disease cases. Our current study will also need to be corroborated further with clinical findings such as verifying regional strain and regional remodeling, which can be a focus in future work.

5. Conclusions

The present work has shown that the inclusion of FSI model can alter the mechanical metrics of the myocardium, relative to running the model as electromechanical configuration alone. Whilst the general trend shows similarity, small differences are noted such as some phase shift and slight difference in magnitude. This is prominent in global metrics such as pressure-volume loop, apex displacement and myocardial torsion. Local metrics such as stress and strain show greater differences in terms of magnitude and phase shift, which likely alter assessment such as regional work. As shown in the results, for cases with nearly uniform myocardial properties, we can expect minimal differences in behavior. However, it is worth noting that in cases where regional differences of myocardial properties are accounted for, such as in infarction, differences between both modelling approaches might be more pronounced.

Acknowledgement

This project has received funding from the Fundamental Research Grant Scheme (FRGS/1/2020/TK0/USMC/02/5) under the auspices of the Malaysian Ministry of Higher Education (MoHE). The authors would like to acknowledge the use of the Iridis 5 HPC facility at the University of Southampton.

Conflict of Interest

The authors declare no conflict of interest

Author Contribution

The authors confirm contribution to the paper as follows: ***study conception and design:*** *Azam Ahmad Bakir, Mohd Jamil Mohamed Mokhtarudin;* ***data collection:*** *Azam Ahmad Bakir;* ***analysis and interpretation of results:*** *Azam Ahmad Bakir, Mohd Jamil Mohamed Mokhtarudin;* ***draft manuscript preparation:*** *Azam Ahmad Bakir, Mohd Jamil Mohamed Mokhtarudin. All authors reviewed the results and approved the final version of the manuscript.*

References

[1] M. J. M. Mokhtarudin, A. Shabudin, and S. Dokos, "Computational Model of Left Ventricle Infarct Remodelling during Passive Filling Phase," in *2018 IEEE-EMBS Conference on Biomedical Engineering and Sciences (IECBES)*, 3-6 Dec. 2018 2018, pp. 166-170, doi: 10.1109/IECBES.2018.8626651.

[2] D. Durrer, R. T. Van Dam, G. E. Freud, M. J. Janse, F. L. Meijler, and R. C. Arzbaecher, "Total Excitation of the Isolated Human Heart," *Circulation,* vol. 41, no. 6, pp. 899-912, June 1, 1970 1970, https://doi.org/10.1161/01.CIR.41.6.899

[3] R. P. Kerckhoffs, M. Neal, Q. Gu, J. Bassingthwaighte, J. Omens, and A. McCulloch, "Coupling of a 3D Finite Element Model of Cardiac Ventricular Mechanics to Lumped Systems Models of the Systemic and Pulmonic Circulation," (in English), *Ann Biomed Eng,* vol. 35, no. 1, pp. 1-18, 2007/01/01 2007, https://doi.org/10.1007/s10439-006-9212-7

[4] S. Göktepe and E. Kuhl, "Electromechanics of the heart: a unified approach to the strongly coupled excitation–contraction problem," (in English), *Comput Mech,* vol. 45, no. 2-3, pp. 227-243, 2010/01/01 2010, https://doi.org/10.1007/s00466-009-0434-z

[5] V. Gurev *et al.*, "A high-resolution computational model of the deforming human heart," (in English), *Biomech Model Mechanobiol,* pp. 1-21, 2015/01/08 2015, https://doi.org/10.1007/s10237-014-0639-8

[6] W. N. W. Ab Naim, M. J. M. Mokhtarudin, B. T. Chan, E. Lim, A. A. Bakir, and N. A. N. Mohamed, "The study of myocardial ischemia-reperfusion treatment through computational modelling," *Journal of Theoretical Biology,* vol. 509, p. 110527, 2021, https://doi.org/10.1016/j.jtbi.2020.110527

[7] W. N. Wan Ab Naim, M. J. M. Mokhtarudin, E. Lim, B. T. Chan, A. Ahmad Bakir, and N. A. Nik Mohamed, "The study of border zone formation in ischemic heart using electro-chemical coupled computational model," *International Journal for Numerical Methods in Biomedical Engineering,* vol. 36, no. 11, p. e3398, 2020, https://doi.org/10.1002/cnm.3398

[8] Y. Hu, V. Gurev, J. Constantino, and N. Trayanova, "Optimizing cardiac resynchronization therapy to minimize ATP consumption heterogeneity throughout the left ventricle: A simulation analysis using a canine heart failure model," *Heart Rhythm,* vol. 11, no. 6, pp. 1063-1069, 6// 2014, http://dx.doi.org/10.1016/j.hrthm.2014.03.021

[9] Y. Alharbi *et al.*, "Fluid structure computational model of simulating mitral valve motion in a contracting left ventricle," *Computers in Biology and Medicine,* vol. 148, p. 105834, 2022/09/01/ 2022, https://doi.org/10.1016/j.compbiomed.2022.105834

[10] A. F. A. Ahmad Azahari, W. N. Wan Ab Naim, N. A. Md Sari, E. Lim, and M. J. Mohamed Mokhtarudin, "Advancement in computational simulation and validation of congenital heart disease: A review," *Computer Methods in Biomechanics and Biomedical Engineering,* pp. 1-14, 2024, https://doi.org/10.1080/10255842.2024.2377338

[11] J. Wong and E. Kuhl, "Generating fibre orientation maps in human heart models using Poisson interpolation," *Computer Methods in Biomechanics and Biomedical Engineering,* vol. 17, no. 11, pp. 1217-1226, 2014/08/18 2012, https://doi.org/10.1080/10255842.2012.739167

[12] L. F. U. Delestri *et al.*, "Modelling of cardiac biventricular electromechanics with coronary blood flow to investigate the influence of coronary arterial motion on coronary haemodynamic," *Computer Methods and Programs in Biomedicine,* vol. 267, p. 108800, 2025/07/01/ 2025, https://doi.org/10.1016/j.cmpb.2025.108800

[13] A. Ahmad Bakir, A. Al Abed, M. C. Stevens, N. H. Lovell, and S. Dokos, "A Multiphysics Biventricular Cardiac Model: Simulations with a Left-Ventricular Assist Device," *Frontiers in Physiology,* vol. 9, p. 1259, 2018.

[14] A. A. Bakir, A. Al Abed, N. H. Lovell, and S. Dokos, "A generic cardiac biventricular fluid-electromechanics model," in *Engineering in Medicine and Biology Society (EMBC), 2017 39th Annual International Conference of the IEEE*, 2017: IEEE, pp. 3680-3683.

[15] T. P. Usyk, R. Mazhari, and A. D. McCulloch, "Effect of Laminar Orthotropic Myofiber Architecture on Regional Stress and Strain in the Canine Left Ventricle," (in English), *Journal of elasticity and the physical science of solids,* vol. 61, no. 1-3, pp. 143-164, 2000/07/01 2000, https://doi.org/10.1023/A:1010883920374

[16] G. A. Holzapfel and R. W. Ogden, "Constitutive modelling of passive myocardium: a structurally based framework for material characterization," *Philosophical Transactions of the Royal Society A: Mathematical, Physical and Engineering Sciences,* vol. 367, no. 1902, pp. 3445-3475, September 13, 2009 2009, https://doi.org/10.1098/rsta.2009.0091

[17] A. G. S. o. B. E. F. o. E. U. Ahmad Bakir, "A multiphysics fluid-electromechanical finite element model of cardiac ventricles for simulation of pathologies and treatments," S. G. S. o. B. E. F. o. E. U. Dokos and N. H. G. S. o. B. E. F. o. E. U. Lovell, Eds., ed, 2018.

[18] L. Agati *et al.*, "Quantitative analysis of intraventricular blood flow dynamics by echocardiographic particle image velocimetry in patients with acute myocardial infarction at different stages of left ventricular dysfunction," *European Heart Journal – Cardiovascular Imaging,* vol. 15, no. 11, pp. 1203-1212, 2014, https://doi.org/10.1093/ehjci/jeu106

[19] N. Westerhof and B. E. Westerhof, "A review of methods to determine the functional arterial parameters stiffness and resistance," *Journal of Hypertension,* vol. 31, no. 9, 2013. [Online]. Available: https://journals.lww.com/jhypertension/fulltext/2013/09000/a_review_of_methods_to_determine_the_functional.3.aspx.

[20] R. E. Henson, S. K. Song, J. S. Pastorek, J. J. H. Ackerman, and C. H. Lorenz, *Left ventricular torsion is equal in mice and humans* (no. 4). 2000, pp. H1117-H1123.

[21] K. Russell *et al.*, "A novel clinical method for quantification of regional left ventricular pressure–strain loop area: a non-invasive index of myocardial work," *European Heart Journal,* vol. 33, no. 6, pp. 724-733, 02/06, 2012, https://doi.org/10.1093/eurheartj/ehs016